Flow Distortion in a Circular-to-Rectangular Transition Duct

J. J. Miau,* T. S. Leu,† J. H. Chou,‡ S. A. Lin†
National Cheng Kung University, Tainan, Taiwan, Republic of China
and
C. K. Lin§
Chung-Shan Institute of Science and Technology, Taichung, Taiwan, Republic of China

Experiments were made for three circular-to-rectangular transition ducts with different transition lengths at Reynolds numbers which ranged from 4×10^3 to 2×10^4. The Reynolds number is based on the inlet boundary-layer thickness and a reference freestream velocity measured upstream of the transition duct. The results indicate that the major driving force for flow in the duct to behave three dimensionally is the cross-streamwise pressure gradient, which results from the contoured wall. A three-dimensional separation bubble was found to occur on the diverging wall at $Re = 4 \times 10^3$, but disappeared at higher Reynolds numbers when the boundary layer upstream of the geometrical deformation section was turbulent. The secondary flow pattern developed at the exit cross-sectional plane was mapped out in detail by a three-dimensional velocity measurement technique. The results further indicated that the development of the secondary flow in the corner region was mainly caused by the mean-flow distortion effect.

Introduction

THE idea of utilizing a rectangular (nonaxisymmetric) exhaust nozzle for the future fighter aircraft engine has been extensively evaluated by a number of investigators[1-4] in recent years. The major advantages of this type of nozzle over the conventional (axisymmetric) one are in the reduction of aerodynamic drag and the enhancement of maneuverability and the thrust reversing ability. However, from the standpoint of engine component integration, a rectangular nozzle needs a circular-to-rectangular transition duct for connection to the afterburner situated upstream because the cross section of a typical afterburner is circular. In principle, this transition duct should be as smooth as possible in order to minimize the flow distortion due to the contoured duct walls; on the other hand, the duct should not be too long since the weight penalty has to be considered. A compromise between these two considerations, therefore, has to be made in designing the duct.

Besides the application mentioned above, a transition section is indispensable in many engineering flow circuits, for instance, the fan-duct integration in a wind-tunnel circuit and the inlet-compressor integration of a fighter gas turbine engine. As a result of its importance in various engineering applications, a number of studies concerning flow through a transition duct have been reported in the literature. Among them the transition models considered are of the shapes of circular to rectangular,[5-7] square to circular,[8] and square to rectangular.[9] It should also be mentioned that a rectangular-to-rectangular transition duct of constant cross-sectional area has often been employed for studying the rapid distortion of a homogeneous turbulent flow.[10,11] In these studies measurements were concerned with the distortion of turbulent intensities in the core region of the duct.

The major emphasis of this study is placed on the possible distortion of flow near the wall in a circular-to-rectangular transition duct. The relevance of the present study to practical considerations can be described in two respects. First, we investigate the possible flow separation which can occur on the diverging wall. This problem is crucial to fighter aircraft applications because the transition duct is installed behind the afterburner, and the nonuniform heat transfer on the wall due to flow separation should be considered. Second, we investigate flow distribution uniformity and the secondary flow pattern at the exit plane of the transition duct. The information obtained is important for one to evaluate the performance of nozzle thrust.

In this study experiments were made under the condition that the inlet flow of the transition duct was uniform in the core region with a thin boundary layer developed on the wall. Thus, the boundary layer grew and became three dimensional in the transition duct, and the flowfield in the potential core, whose size varied inversely with the thickness of the boundary layer, was distorted.

Experimental Method

Wind Tunnel

The test section of the low-speed wind tunnel employed in this study, shown in Fig. 1, is composed of a circular duct 503 mm in diameter and 500 mm in length, a transition duct, and a rectangular duct 150 mm in length. At the inlet section of the transition duct, the streamwise turbulence intensity measured in the core region was about 0.3%, and the velocity distribution in the core region was verified to be reasonably uniform. For instance, at $U_0 = 35.5$ m/s where U_0 denotes the velocity measured in the core region at a reference point located 25 cm upstream of the transition duct, the difference between the maximum and the minimum velocities measured in the core region was about 1.4% of U_0.

In this study, (U,u), (V,u), and (W,w) denote the time-averaged velocities and the instantaneous fluctuating velocities in the x, y, and z directions, respectively, where x, y, and z are the orthogonal axes shown in Fig. 1.

Transition Models

Three transition models were selected for this study. The geometry of each model was determined according to the following rules.

1) The cross-sectional area was held constant throughout the duct.

2) The aspect ratio of the rectangular cross section at the exit plane was 2 with dimensions of 630.5 × 315.2 mm.

Received Jan. 30, 1989; revision received Nov. 3, 1989.

*Associate Professor, Institute of Aeronautics and Astronautics. Member AIAA.
†Graduate Student, Institute of Aeronautics and Astronautics.
‡Associate Professor, Department of Engineering Sciences.
§Senior Scientist.

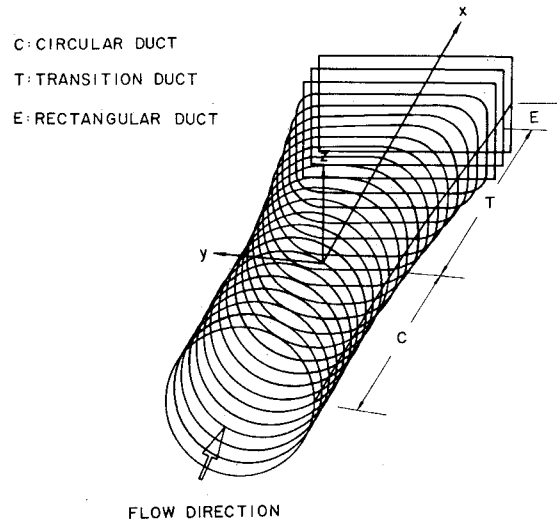

Fig. 1 Schematic view of the test section and the coordinate system.

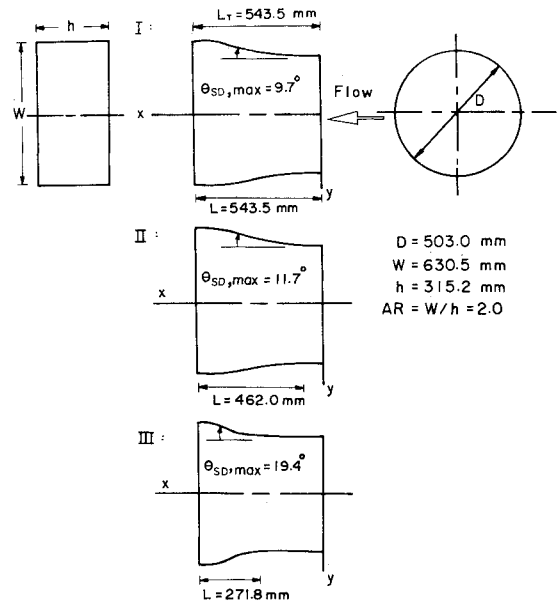

Fig. 2 Shapes of the diverging walls of the transition models.

3) The curved surface of the diverging wall of each model was determined by a third-order polynomial; see Fig. 2 for the shape of the diverging walls of each of the models.

4) A 90-deg circular arc was adopted to smooth the corner of the duct. The radius of the circular arc r was determined by the relation

$$\frac{r}{R} = (1 - x/L)^p; \qquad p = \frac{1}{2}$$

where

R = the radius of the inlet circular cross section, which is 251.5 mm

x = the streamwise distance measured from $x = 0$, the location in the transition duct where the geometrical change starts

L = the geometrical transition length, which should be distinguished from L_T, the total length of the transition duct; in the cases of models II and III, L_T is greater than L (see Fig. 2)

5) The shape of the converging wall was determined by the constraints 1–4 given above.

6) The transition length ratios $L/2R$ of the three models, called I, II, and III, were 1.08, 0.92, and 0.54, respectively.

Each of the models was made of plexiglass and manufactured by a numerical-control machine. The contour of the inner polished surface was within ± 0.1 mm in precision.

Pressure and Velocity Measurement Techniques

Wall pressure measurements were obtained from static pressure holes, 0.8 mm in diameter, drilled into the wall surface of each model. For model I the number of holes drilled into one quadrant of the wall surface is 170; while for models II and III, they are 150 and 90, respectively. A Validyne DP-103 differential-type pressure transducer was employed to measure the time-mean pressure at each of the static taps. The output voltage of the pressure transducer was calibrated by means of a micromonameter with a resolution of ± 0.05-mm water, prior to performing the experiments.

Velocity measurements were made using DANTEC 55M01 hot-wire anemometers. The hot-wire probe (either a normal or a cross-wire probe) was inserted from downstream of the test section and was mounted on a two-dimensional tranversing mechanism. The traversing mechanism was equipped with two stepping motors controlled by a 16-bit personal computer. Thus, velocity measurements at each cross-sectional plane in the transition duct could be performed automatically. The movement of the velocity probe in the longitudinal direction, however, was made manually. This led to some difficulties in the boundary-layer velocity profile measurements, which will be mentioned later. For the measurements of secondary flow pattern at the exit cross-sectional plane, a technique similar to that described by Shabaka et al.[12] was employed. By rotating the cross-wire probe for 45 and 90 deg consecutively at the same point the mean velocities in three perpendicular directions and the Reynolds stresses could be obtained.

Flow Symmetry Consideration

Preliminary measurements using a pitot tube probe to survey the mean flow distribution in each of the transition models indicated that flow in the duct was symmetric with respect to the x-z and x-y planes (see Fig. 1 for the coordinate system). Hence, measurements were basically made in one quadrant of the model, and the results obtained were interpreted for the entire flowfield. The quadrant chosen for measurement was in the upper-right portion of the duct flow, as viewed from downstream of the transition model.

Results and Discussions

Wall Pressure Distribution

The cross-sectional wall pressure distributions of models I and III obtained at $U_0 = 6.1$ m/s, 21.1 m/s, and 35.5 m/s are shown in Figs. 3 and 4, respectively. In each of the plots, the vertical scale represents the magnitude of the pressure coefficient C_p, which is defined as

$$C_p = \frac{P - P_0}{\frac{1}{2}\rho U_0^2}$$

Here P_0 is the reference wall static pressure measured at 25 cm upstream of the inlet of the transition duct. The horizontal scale represents the normalized circumferential distance, c'/s, where c' is the distance measured from the corner location dividing the side (diverging) wall and top (converging) wall and $s = \pi R/2$ is a normalization factor. The single and double arrow symbols marked on the horizontal axis indicate the centerline positions of the diverging wall and the converging wall, respectively.

Three noticeable features are observed from the figures. First, a comparison of the C_p distributions obtained at differ-

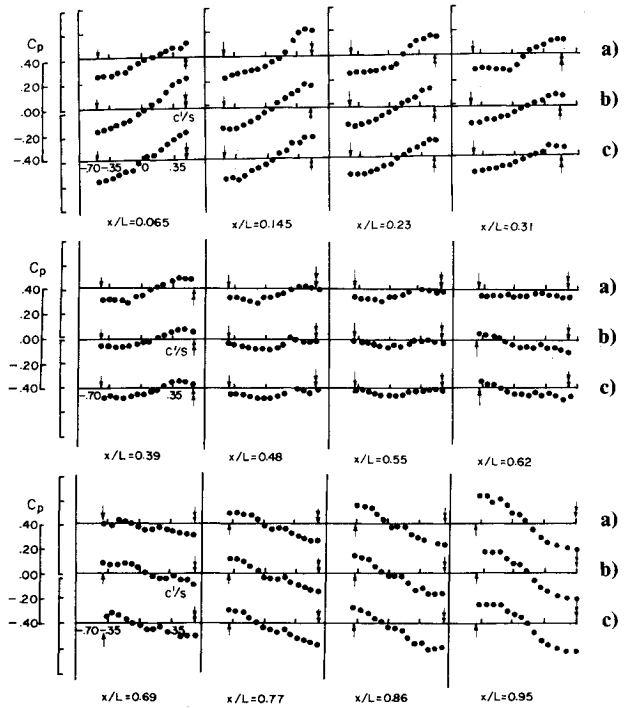

Fig. 3 Cross-streamwise wall pressure distributions of model I at a) $U_0 = 6.1$ m/s; b) $U_0 = 21.1$ m/s; and c) $U_0 = 35.5$ m/s.

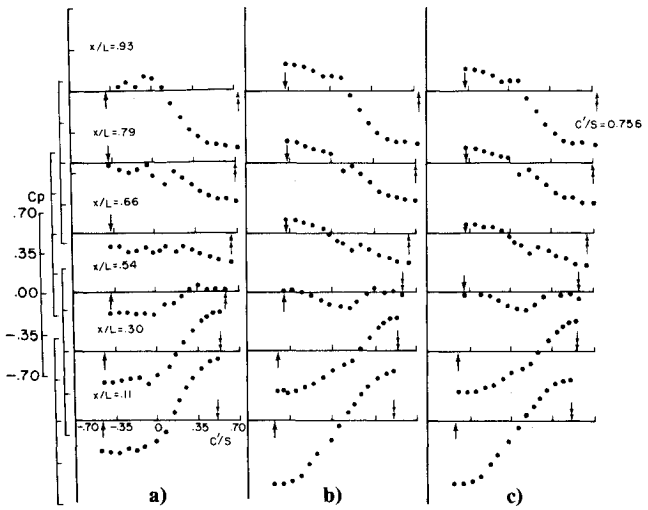

Fig. 4 Cross-streamwise wall pressure distributions of model III at a) $U_0 = 6.1$ m/s; b) $U_0 = 21.1$ m/s; and c) $U_0 = 35.5$ m/s.

ent cross sections reveals that the wall pressure distribution in a transition duct is three dimensional in nature. In the region upstream of $x/L = 0.55$ to 0.62, the pressure measured on the side wall is lower than that measured on the top wall; while in the region further downstream, the situation is reversed. Consequently, flow near the side wall is subjected to an adverse pressure gradient in the streamwise direction; whereas flow near the top wall experiences a favorable pressure gradient. The wall pressure variation seen at the exit plane follows the same trend as that reported by Patrick and McCormick[7] for flow through a circular-to-rectangular transition duct of aspect ratio 3. Second, for each of the models, at each of the streamwise locations where data were taken, the C_p distributions corresponding to $U_0 = 21.2$ m/s and 35.5 m/s almost coincide; while the C_p distributions for $U_0 = 6.1$ m/s behave somewhat differently, for instance see Fig. 4 for the C_p distributions obtained downstream of $x/L = 0.30$ in the region of $c'/s < 0$. The peculiar behavior seen in the C_p distributions of $U_0 = 6.1$ m/s will be further explained later. Third, it is seen that the magnitude of pressure variation in a single cross-sectional plane varies with the models studied. For model I the difference of the C_p values measured in a cross-sectional plane is no more than 0.4; while for model III, it can be as much as 0.8.

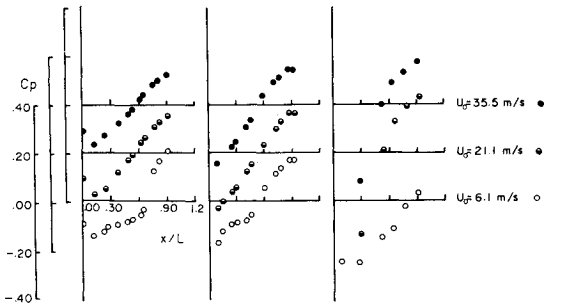

Fig. 5 Pressure distributions along the centerline of the diverging walls of the three models at $U_0 = 6.1$, 21.1, and 35.5 m/s.

The feature of pressure varying in the cross-stream direction in the transition duct deserves further discussion here. In the upstream half region of the duct, the converging wall is concave in the streamwise direction, thus, producing a positive pressure gradient in the direction normal to the curved surface, i.e., pointing into the wall surface; while the diverging wall is convex, thus, producing a negative pressure gradient. If one takes the pressure at the center of the duct as a reference, it is evident that the pressure measured on the converging wall is higher while the pressure measured on the diverging wall is lower. In the downstream half of the transition duct, the situation seen in Figs. 3 and 4 is reversed. Again, this is due to the contours of the diverging and converging walls being in concave and convex shapes, respectively. This explanation also implies that the formation of the cross-streamwise pressure gradient in a transition duct is due to the contour of the wall.

Comparison of the C_p distributions obtained at different streamwise locations indicates that the streamwise adverse pressure gradient developed along the centerline of the diverging wall is much more severe than that developed in any other portion of the duct. To illustrate this effect, the C_p values obtained along the centerline of the diverging wall are replotted in Fig. 5. It is seen in this figure that for all three models, at $U_0 = 21.1$ m/s and 35.5 m/s, static pressure increases with x/L almost linearly; while at $U_0 = 6.1$ m/s, the C_p distributions for models I and II show that a flattened region occurs approximately from $x/L = 0.3$ to 0.5 and that the C_p distribution for model III does not increase until downstream of $x/L = 0.3$. These trends seen at $U_0 = 6.1$ m/s, together with the previous observations in Figs. 3 and 4 for the cross-streamwise pressure variations under the same U_0 condition, lead one to speculate that the flow is separated from the diverging wall within a certain region. The experimental evidence to support this is presented and discussed below.

In the present wind-tunnel study, a tuft method was used to sense the flow direction in the near-wall region. The visualizations obtained along the centerline of the diverging wall revealed that at $U_0 = 6.1$ m/s, the flow direction was indeed reversed in the regions shown in Fig. 5 where the wall pressure distribution is flattened. A more illustrative view of this phenomenon was provided by the water-tunnel experiments with a transition model (model II) of a smaller size at a Reynolds number comparable to that of the wind-tunnel experiment at $U_0 = 6.1$ m/s. Pictures obtained[13] from the side and end views of this transition model are reproduced in Fig. 6, showing that as the dye streaks reach the midsection of the

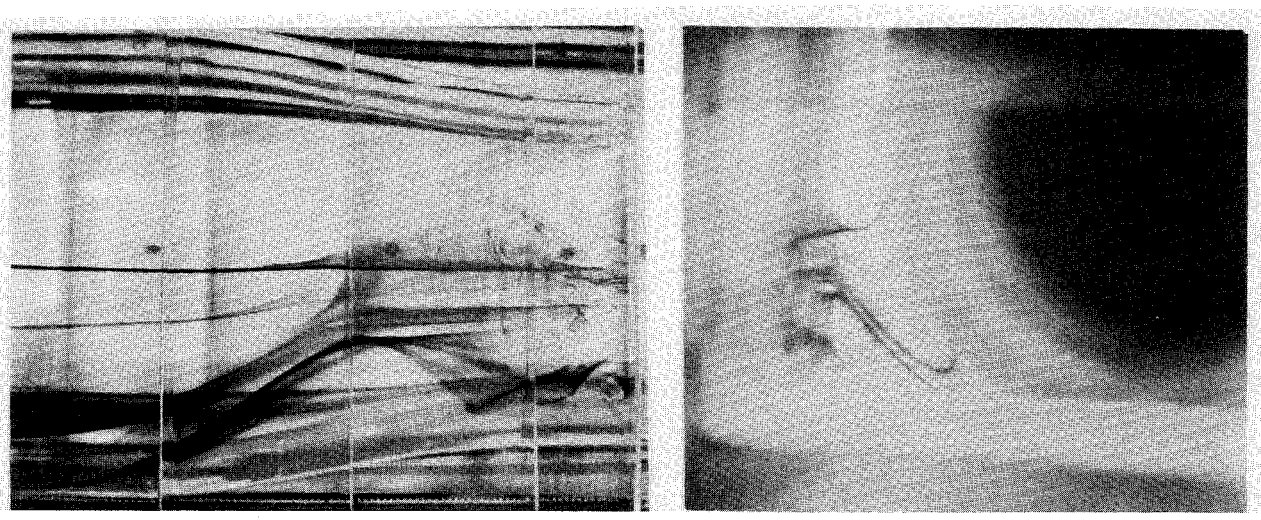

Fig. 6 Dye visualizations of flow near the wall of model II at $Re = 3.14 \times 10^3$. Ref. 13.

duct, they diffuse abruptly with a small portion of dye reversing upstream. Referring to the sketch included in the figure, one can further interpret that the abrupt diffusion of dye is caused by the dye reaching the leading edge of the separation bubble situated on the diverging wall. The forefront of the separation bubble is suggested to be a point of singular separation,[14] from which the separation lines extend toward the corner regions. It should be pointed out that the dye streak pictures and the sketch presented in Fig. 6 do not show the reattaching process of the separation bubble clearly. From the tuft visualizations performed in the wind tunnel, one could roughly estimate that for models I and II, the flow reattached to the diverging wall at $x/L = 0.5$ and for model III, the flow separation bubble persisted throughout the duct. These observations are consistent with the appearances of the C_p distributions for $U_0 = 6.1$ m/s shown in Fig. 5.

The dye streaks seen in the pictures indicate that flow near the wall does not convect in the streamwise direction; instead, it curves from the bottom wall to the side wall in the upstream half region of the transition duct (see also the sketch given in Fig. 6). This skewing tendency coincides with the behavior of the cross-streamwise pressure gradient depicted in Figs. 3 and 4. It is caused by the flow very near the wall being dominated by the pressure gradient effect, as the convective terms in the momentum equation are comparatively small in the near-wall region.

Boundary Layer Developed along the Centerline of the Diverging Wall

Assuming that flow in the boundary layer is parallel to the wall, and that at the centerline of the diverging wall the vertical component of the mean velocity is zero (by symmetry considerations), we employed a normal hot-wire probe to perform velocity measurements in the boundary layer. The results for model I under the conditions of $U_0 = 6.1$ m/s, 21.1 m/s, and 35.5 m/s are shown in Fig. 7. The results corresponding to the other two models are found to be similar to those shown in Fig. 7 and are therefore not shown here. It should be mentioned that the velocity profiles shown in Fig. 7 are not measured in the direction normal to the wall but along the y direction. This is due to the manner in which our two-dimensional traversing mechanism was operated. However, since the boundary-layer thickness is much smaller than the radius of curvature of the diverging wall, the velocity profiles shown in the figure can be taken as the boundary-

layer profiles measured along the direction normal to the wall providing that the boundary-layer thickness is corrected by a cosine factor to account for the angle between the y axis and the local surface normal.

The data in Fig. 7 provide information on the boundary-layer thickness at $x/L = 0$, denoted as δ_0 for $U_0 = 6.1$, 21.1, and 35.5 m/s, respectively. The Reynolds number, defined as $U\delta_0/\nu$, is about 4×10^3 for $U_0 = 6.1$ m/s and is about 2×10^4 for $U_0 = 35.5$ m/s. In this study our main interests are on the flow phenomena near the wall; therefore, it is proper to choose δ_0 as the characteristic length scale.

Figure 7a shows that the velocity profiles obtained at $U_0 = 6.1$ m/s are severely distorted in the streamwise region from $x/L = 0.3$ to 0.5. This is the region where the three-dimensional separation bubble occurs. The cross-sectional shape of the separation region, as determined from the tuft visualizations, is also indicated in the figure by the dashed line. Downstream of $x/L = 0.5$, the velocity profiles are gradually relaxed to a smooth shape signifying that flow reattaches on the wall.

The velocity profiles obtained at $U_0 = 21.1$ m/s and 35.5 m/s, shown in Figs. 7b and 7c, respectively, give no indication of flow separation on the wall. It is also found that the difference in the boundary-layer thickness of these two cases is insignificant. This explains why the wall pressure distributions of these two cases shown in Fig. 3 are similar, as can be reasoned from the point of view of a boundary-layer displacement effect.

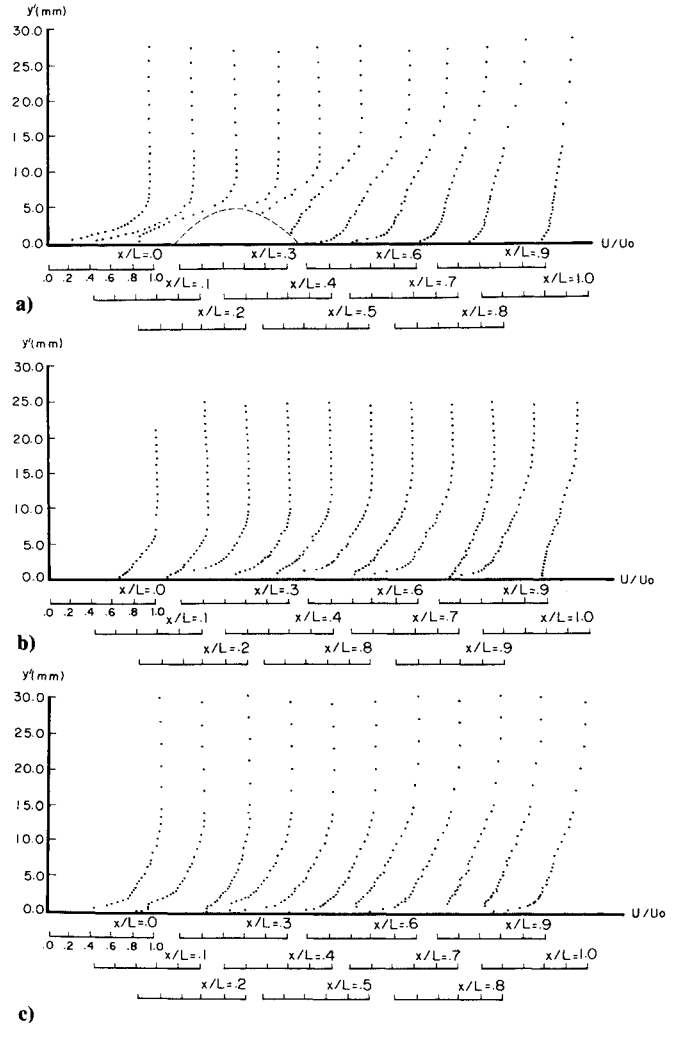

Fig. 7 Boundary-layer profiles along the centerline of the diverging wall of model I: a) $U_0 = 6.1$ m/s; b) $U_0 = 21.1$ m/s; and c) $U_0 = 35.5$ m/s.

The shape factor values corresponding to the velocity profiles shown in Fig. 7 are calculated and presented in Fig. 8. Note that by definition the shape factor is the ratio of the displacement thickness to the momentum thickness. Therefore, the cosine factor mentioned previously for correcting the boundary-layer thickness does not appear in the shape factor value. First, we should like to examine the shape factor distributions obtained at $U_0 = 6.1$ m/s, as shown in Fig. 8a. In this figure a number of the data points are encircled with dotted lines, which indicates that the values were obtained in the separated flow region and are therefore for reference only. Immediately upstream of the separation region, the shape factor values can be higher than 3, which are comparable to the value obtained in a two-dimensional laminar layer on the verge of separation.[15] Downstream of the separation region, the shape factor values for models I and II decrease monotonically along x/L and reach 1.4–1.6 at $x/L = 1$. These values suggest that downstream of the separation bubble the boundary layer becomes turbulent and approaches flat-plate behavior at the exit plane.[15] For model III, the separation bubble persists until the end of the transition section; therefore no data points are plotted in the region downstream of $x/L = 0.3$.

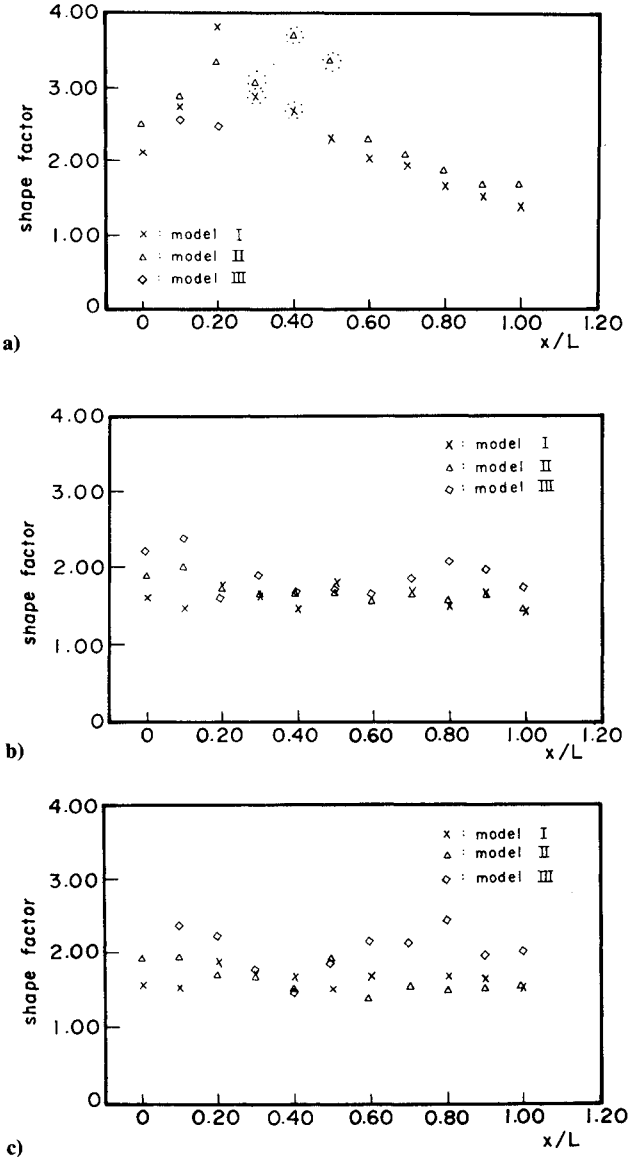

Fig. 8 Shape factor distributions along the centerline of the diverging wall: a) $U_0 = 6.1$ m/s; b) $U_0 = 21.1$ m/s; and c) $U_0 = 35.5$ m/s.

In Figs. 8b and 8c, it is seen that the shape factor values obtained at $U_0 = 21.1$ m/s, and 35.5 m/s fall in a range between 1.4 and 2.4 throughout the transition duct; although the shape factor values for model III appear to be higher than the values for models I and II. This behavior is clearly different from that seen in Fig. 8a. Also, it can be noted that these shape factor values are comparable to those obtained in a two-dimensional turbulent boundary layer under an adverse pressure gradient.[15] Therefore it is suggested that under the conditions of $U_0 = 21.1$ m/s and 35.5 m/s, the boundary layer is turbulent throughout the transition duct. Previous measurements of the streamwise turbulent intensity using a normal hot-wire probe[16] also confirm that at $U_0 = 21.1$ m/s and 35.5 m/s, the maximum turbulent intensity measured at each streamwise location in the boundary layer can reach 8 to 9% or even higher.

The shape factor distributions presented in Fig. 8 readily explain why the boundary layer separates from the diverging wall of the duct at $U_0 = 6.1$ m/s but not so at $U_0 = 21.1$ m/s and 35.5 m/s. The fact is that at $U_0 = 6.1$ m/s the boundary layer at $x/L = 0$ is not turbulent. Hence, the downstream flow tends to separate from the diverging wall of the transition duct; while at $U_0 = 21.1$ m/s and 35.5 m/s, the boundary layer at $x/L = 0$ is turbulent already and is therefore capable of overcoming the adverse pressure gradient developed downstream.

Flow Characteristics at the Exit Plane

The normalized equistreamwise velocity (U/U_0) contours obtained at the exit plane for models I and III at $U_0 = 6.1$ m/s are shown in Fig. 9, where it is seen that the region of maximum velocity is situated close to the converging wall. This behavior appears to be associated with three-dimensional distortion of flow in the core region; that is, the streamwise velocity increases from the center of the core to the converging walls while it decreases from the center of the core to the diverging walls. Comparison of the plots presented in this figure also indicates that the maximum velocity varies with U_0 as well as with transition length. It is plausible that the deviation of the maximum value from 1 can be taken as an indication of the distortion of the mean flow. A practical definition called the effective blockage fraction[7,17] is adopted here for quantifying the distortion of the velocity distribution. According to Sovran and Klomp,[17] the effective blockage fraction can be expressed as

$$B = 1 - E$$

where E is called the effective area fraction, defined as U_{av}/U_{max}. Here U_{av} denotes the average (bulk) velocity and U_{max} denotes the maximum velocity measured at the exit plane. U_{av} is taken to be U_0 because the boundary-layer thickness upstream of the transition duct is thin and negligible compared to the diameter of the circular duct. The presently measured results for the case of $U_0 = 35.5$ m/s, model I, give the lowest B value of 0.048 and the highest B value (0.167) for the case of $U_0 = 6.1$ m/s, model III.

The equistreamwise turbulent intensity ($\sqrt{\overline{u^2}}/U_0$) contours obtained at the exit cross-sectional plane are also plotted in Fig. 10. It is seen that in each of the cases, the turbulent intensity measured in the core region is low, about 0.3–0.4%, which is comparable to the turbulence level measured in the core region upstream of the transition duct. This behavior substantiates the claim that the nonuniform velocity distribution developed in the core region is mainly caused by the contour of the duct. Thus, turbulent transport effects are not involved. Recently Burley and Carlson[18] made calculations of flow in a circular-to-rectangular transition duct based on the assumption of irrotational flow. The present findings indicate that their approach is appropriate provided that the detailed flow behavior near the wall is not of interest. It should be mentioned that in this study no detailed measurements were made for the turbulent intensity in the core region. Therefore, the study of distortion associated with a homogeneous turbulent flow is beyond the present scope.

The secondary flow structures which developed in the corner region of the transition duct were investigated in detail by using the three-dimensional velocity measurement technique described earlier. These flow structures can be revealed from a cross-streamwise, two-dimensional velocity vector plot. As an example, a plot obtained by this technique for mode III at $U_0 = 35.5$ m/s is shown in Fig. 11. This figure shows that the secondary flow structure developed in the corner region rotates in the counterclockwise sense. Interestingly, this sense of rotation can also be deduced from the behavior of the wall

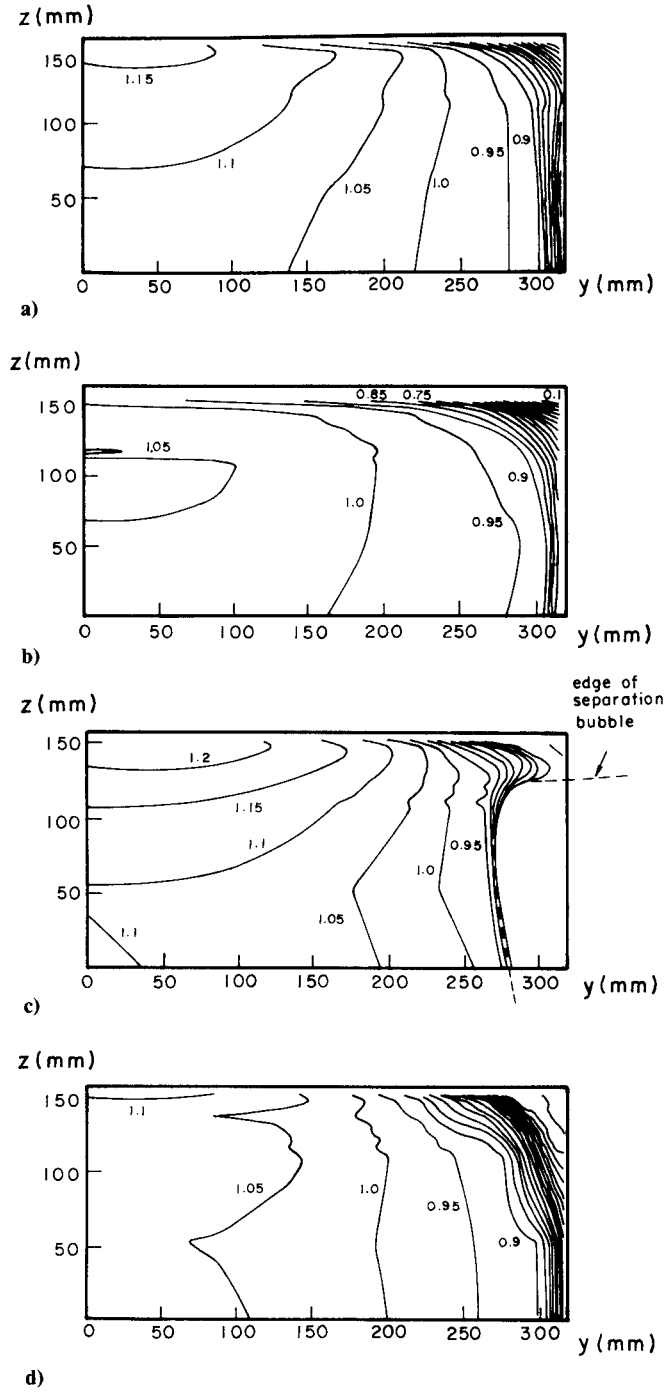

Fig. 9 Equistreamwise velocity contours (U/U_0) at the exit plane of the transition models: a) model I, $U_0 = 6.1$ m/s; b) model I, $U_0 = 35.5$ m/s; c) model III, $U_0 = 6.1$ m/s; and d) model III, $U_0 = 35.5$ m/s.

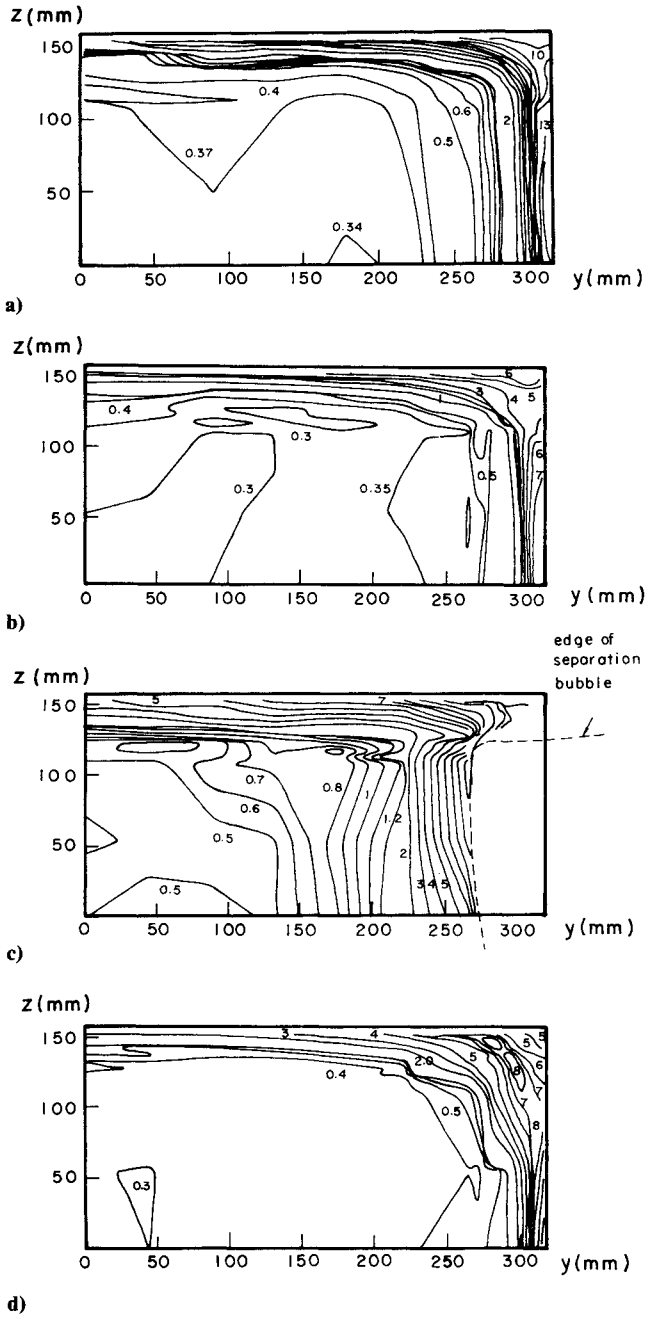

Fig. 10 Equistreamwise turbulence intensity $[(\sqrt{\overline{u^2}}/U_0) \times 100]$ contours at the exit plane of the transition models: a) model I, $U_0 = 6.1$ m/s; b) model I, $U_0 = 35.5$ m/s; c) model III, $U_0 = 6.1$ m/s; and d) model III, $U_0 = 35.5$ m/s.

pressure distributions shown in Fig. 4. From Fig. 4 one learns that near the exit plane $x/L = 1$ the pressure measured on the side wall is greater than the pressure measured on the top wall; therefore, flow near the wall is dominated by the pressure gradient effect. Meanwhile, flow away from the wall due to the three-dimensional distortion of the potential core shows a tendency to convect from the top wall to the side wall. As a result, a counterclockwise rotation motion is formed in the corner region. The mechanism of pressure gradient driven secondary flow was discussed by Towne and Schum[19] in the study of flow through an S-shaped duct. They explained that the secondary flow pattern within the boundary layers along the top and bottom walls near the side wall was due to the countour of the S-shaped duct which led to buildup of the cross-stream pressure gradient.

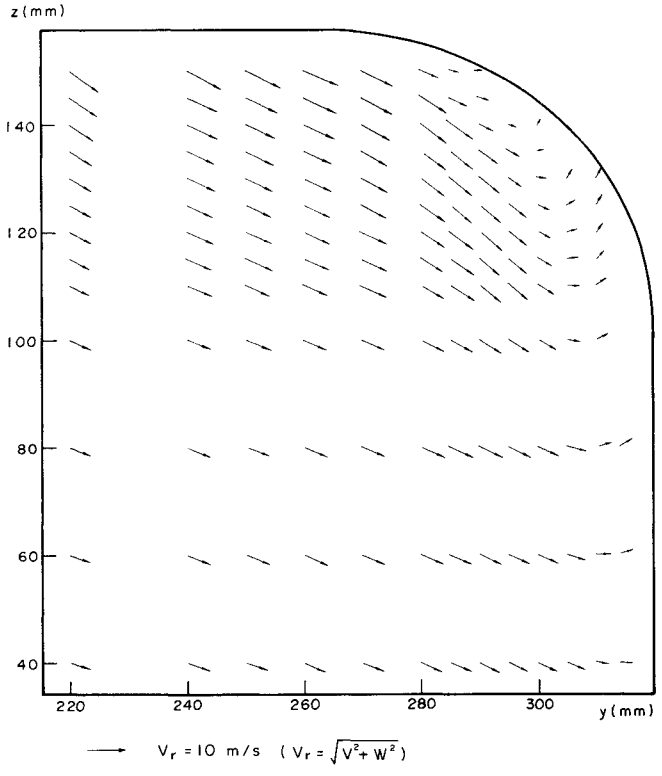

Fig. 11 The V-W velocity vector diagram for $U_0 = 35.5$ m/s, see model III, at 1 cm upstream of the exit cross-sectional plane.

The maximum crossflow seen in Fig. 11, outside the circulation region, is of the magnitude about $0.2U_0$. This value is found to be higher than that reported by Patrick and McCormick[7] for flow through a transition duct with an aspect ratio of 3 at the exit cross section. The discrepancy could be due to the streamwise measuring locations, which were different for the two experiments. The data shown in Fig. 11 were obtained 1 cm upstream of the exit plane; while the data presented by Patrick and McCormick[7] were obtained slightly downstream of the exit plane.

Vorticity dynamics can be applied to explore the mechanisms responsible for the development of the secondary flow in the corner region. It is known that the secondary flow phenomenon is associated with the streamwise vorticity embedded in the flow,[20] and the steady, mean streamwise vorticity equation can be written in the following form.[21]

$$U\frac{\partial \Omega_x}{\partial x} + V\frac{\partial \Omega_x}{\partial y} + W\frac{\partial \Omega_x}{\partial z} = \underset{(1)}{\Omega_x\frac{\partial U}{\partial x}} + \underset{(2)}{\Omega_y\frac{\partial U}{\partial y}} + \underset{(3)}{\Omega_z\frac{\partial U}{\partial z}}$$

$$+ \underset{(4)}{\frac{\partial}{\partial x}\left(\frac{\partial \overline{uv}}{\partial z} - \frac{\partial \overline{uw}}{\partial y}\right)} + \underset{(5)}{\left(\frac{\partial^2}{\partial y^2} - \frac{\partial^2}{\partial z^2}\right)(-\overline{vw})}$$

$$+ \frac{\partial^2}{\partial y\,\partial z}(\overline{v^2} - \overline{w^2}) + \nu\nabla^2\Omega_x$$

Here Ω_x, Ω_y, and Ω_z, are the mean vorticities and velocity fluctuations in the x, y, and z directions, respectively; ν is the kinematic viscosity. From the equation it is seen that the vorticity change of a fluid element is primarily due to two mechanisms: one is stretching [term 1] and tilting [terms 2 and 3] by the mean flow, and the other is the turbulent transport effect [terms 4, 5, and 6]. For the secondary flow developed in the corner region of a transition duct, it is not obvious which of the mechanisms is more important. Hence, an evaluation of these two mechanisms based on the experimental data ob-

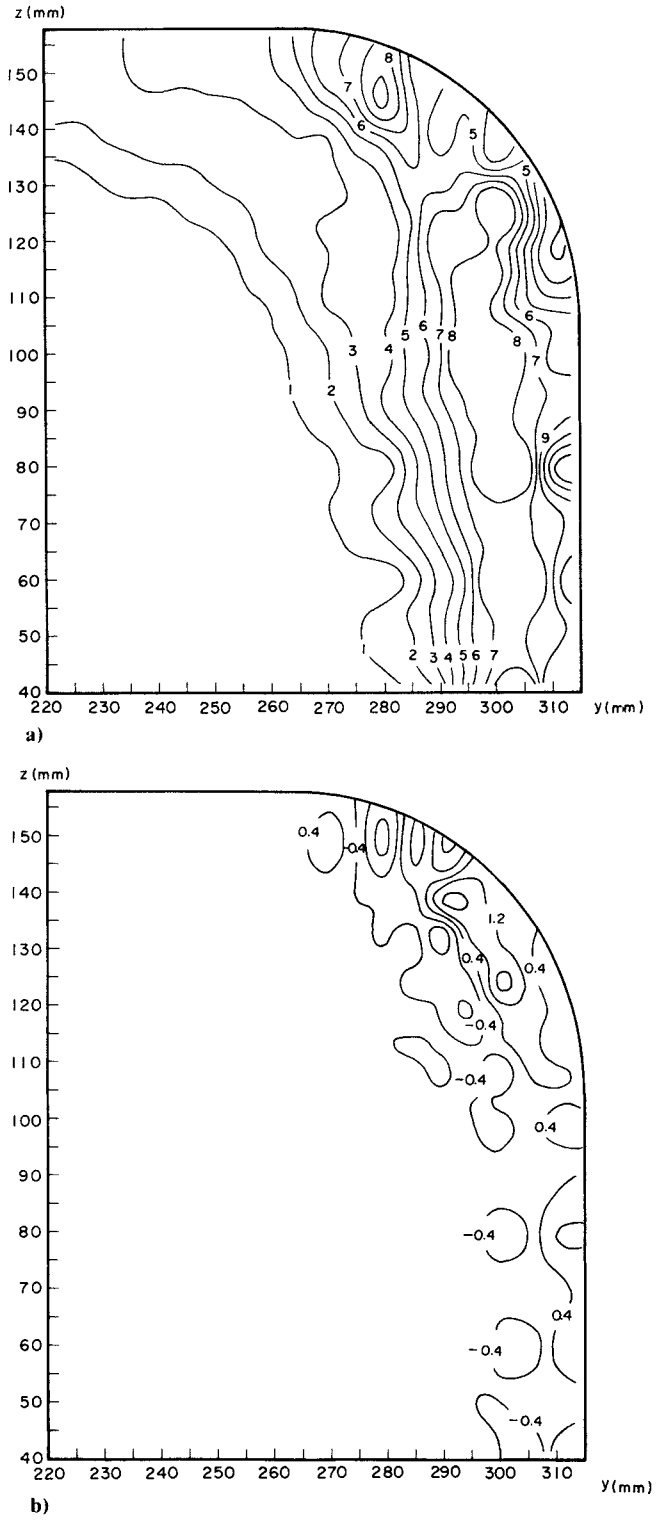

Fig. 12 Contours corresponding to the magnitude of a) the mean flow distortion terms [including terms 1, 2, and 3 in the vorticity equation]; b) the turbulent transport terms [including terms 4, 5, and 6 in the vorticity equation], in the corner region of model III, $U_0 = 35.5$ m/s; the values shown are normalized by U_0^2/R^2.

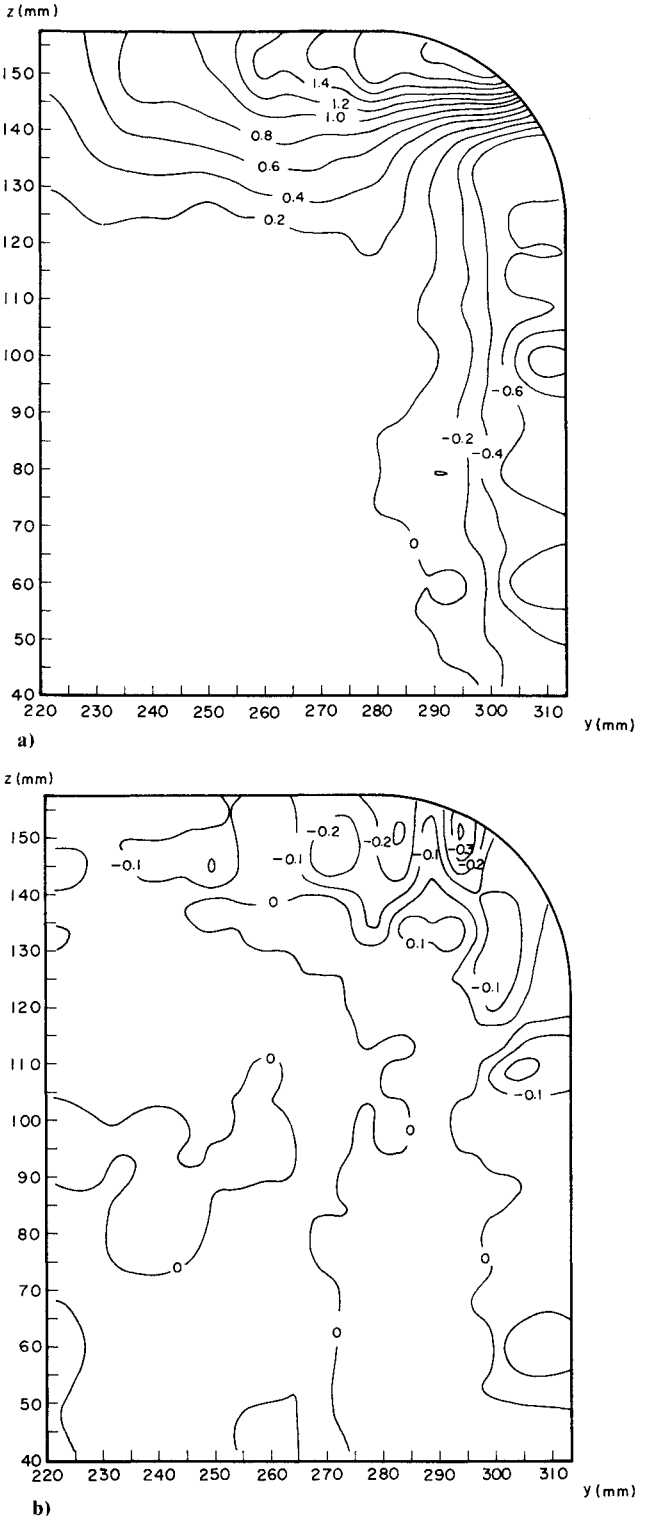

Fig. 13 Contours corresponding to the magnitude of a) the mean-flow distortion terms, including terms 1, 2, and 3 in the vorticity equation; b) the turbulence transport terms, including terms 4, 5, and 6 in the vorticity equation, in the corner region of model I, $U_0 = 35.5$ m/s; the values shown are normalized by U_0^2/R^2.

tained is necessary. Calculation procedures were carried out with a finite-difference scheme using two sets of data obtained at the exit plane and a cross-sectional plane 1 cm upstream of the exit plane, respectively. All the quantities indicated by terms 1–6 of the equation were therefore estimated. The calculated results for model III at $U_0 = 35.5$ m/s are shown in Fig. 12, which clearly shows that in the corner region, the magnitude of the sum of the mean flow distortion terms (see Fig. 12a) is at least four times greater than the sum of the turbulent transport terms (see Fig. 12b). This comparison substantiates that the mean-flow distortion effect, which is mainly due to the geometrical contour of the duct, is dominant over the the turbulent transport effect. Similarly, the calculated results for model I at $U_0 = 35.5$ m/s are presented in Fig. 13, which also shows that the mean-flow distortion effect is dominant over the turbulent transport effect. In

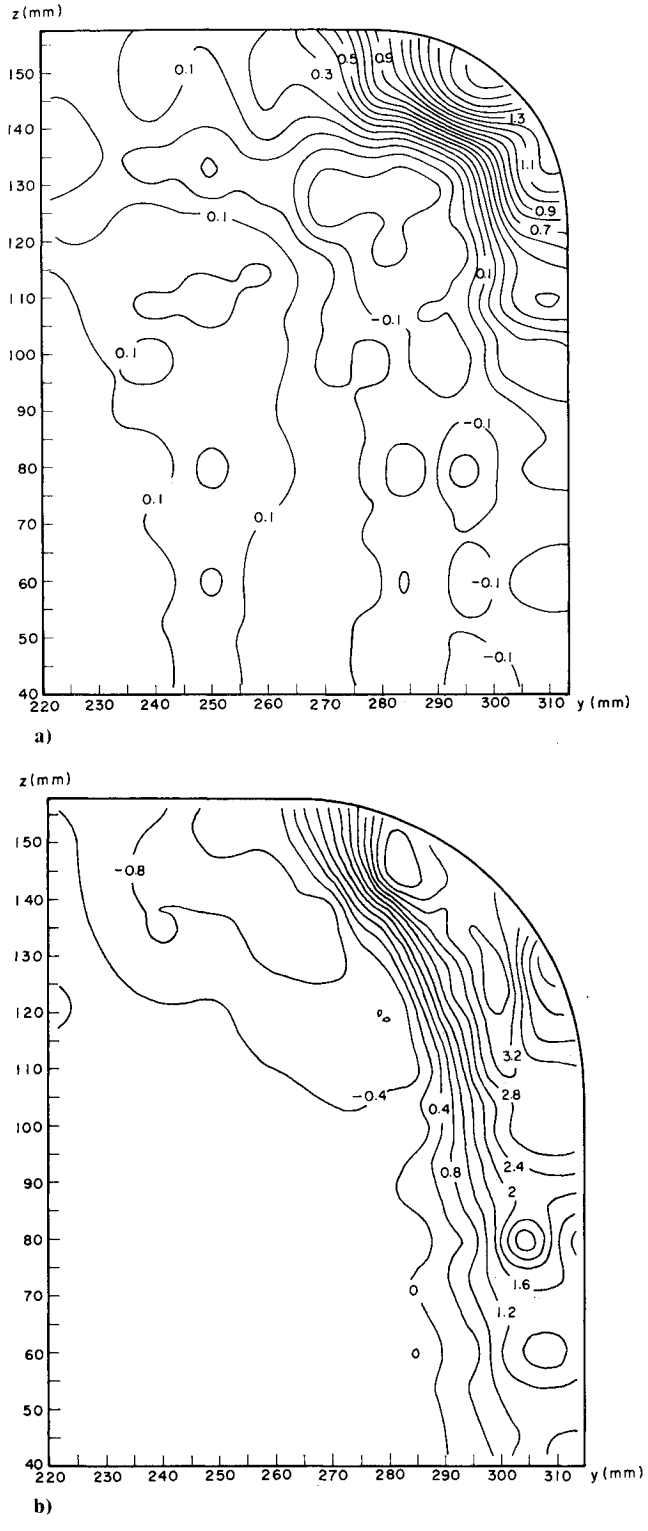

Fig. 14 Nondimensional streamwise vorticity contours in the corner region of a) model I, $U_0 = 35.5$ m/s; b) model III, $U_0 = 35.5$ m/s; the vorticity values are normalized by U_0/R.

general, the present results illustrate that in a contoured duct the streamwise vorticity generated by the mean-flow distortion effect is much more pronounced than vorticity generated by turbulent transport. This result is similar to the findings of Taylor et al.,[8] who studied the flow in a square-to-circular transition duct. This finding is different from that for the case of flow through a straight rectangular duct,[21] where the secondary flow which develops in the corner region is due primarily to the anisotropic turbulence effect.

Comparison of Figs. 12 and 13 further indicates that the magnitude of the mean-flow distortion terms for model III is much larger than that for model I. This is attributed to the fact that the transition length of model III is shorter than that of model I; therefore, the distortion rate of the mean flow in model III is higher. Correspondingly, it is expected that the strength of the secondary flow developed in model III should be higher than that developed in models I or II. To confirm this argument, the normalized equistreamwise vorticity contours reduced from the mean velocity data obtained in the corner regions of models I and III, at $U_0 = 35.5$ m/s, 1 cm upstream of the exit plane, are presented in Fig. 14 for comparison. As seen in this figure, the streamwise vorticity contained in the secondary flow structure of model III is about three to five times that of model I. It is also found that the strength of the streamwise vorticity increases as the measured position approaches the wall of the corner. This feature shows that flow in the corner region is strongly three-dimensional in nature.

Conclusions

In this study the three-dimensional nature of flow in a circular-to-rectangular transition duct has been investigated. The cross-streamwise pressure gradient which results from the contoured wall drives the near-wall flow from the converging wall to the diverging wall in the upstream half region of the transition model and reverses the situation further downstream. The streamwise adverse pressure gradient developed along the diverging wall causes a separation bubble to form at $Re = 4 \times 10^3$ but does not lead to its formation at higher Reynolds numbers. This difference is attributed to the observation that the boundary layer is turbulent at the inlet of the transition duct at higher Reynolds numbers. Therefore, the flow is capable of overcoming the adverse pressure gradient downstream. The velocity measurements obtained at the exit plane suggest that the secondary flow structure developed in the corner of the transition duct is mainly caused by the mean flow distortion effect. As the transition length is shortened, the strength of the secondary vortex developed in the corner region increases.

Acknowledgments

The financial support from the National Defense Technology Coordination Council, Republic of China, on this work is gratefully acknowledged. The first author (JJM) would like to thank L. S. Yao (Arizona State University) for discussion on the mechanisms responsible for the generation of secondary flow.

References

[1]Willard, C. M., Capone, F. J., Konarski, M., and Stevens, H. L., "Static Performance of Vectoring/Reversing, Nonaxisymmetric Nozzle," *Journal of Aircraft*, Vol. 16, 1979, pp. 116–123.

[2]Bowers, D. L., "Aerodynamic Effects Induced by a Vectored High Aspect Ratio Nonaxisymmetric Exhaust Nozzle," *Journal of Aircraft*, Vol. 16, 1979, pp. 515–520.

[3]Laughrey, L. A., Drape, D. J., and Hiley, P. E., "Performance Evaluation of an Air Vehicle Utilizing Nonaxisymmetric Nozzle," *Journal of Aircraft*, Vol.18, 1981, pp. 89–95.

[4]Stevens, H. L., Thayer, E. B., and Fullerton, J. F., "Development of the Multifunction 2-D/C-D Nozzle," AIAA Paper 81-1419, 1981.

[5]Mayer, E., "Effect of Transition in Cross-Sectional Shape on the Development of the Velocity and Pressure Distribution of the Turbulent Flow in Pipes," NACA TM903, 1939.

[6]Patrick, W. P., and McCormick, D. C., "Circular-to-Rectangular Duct Flows—a Benchmark Experimental Study," SAE TP-871776, Aerospace Technology Conference and Exposition, Long Beach, CA, Oct. 1987.

[7]Patrick, W. P., and McCormick, D. C., "Laser Velocimeter and Total Pressure Measurements in Circular-to-Rectangular Transition Ducts," NASA CR-182286, 1988.

[8]Taylor, A. M. K. P., Whitelaw, J. H., and Yianneskis, M., "Turbulent Flow in a Square to Round Transition," NASA CR 3447, 1981.

[9]Dekam, E. I., and Calvert, J. R., "Effects of Inlet Conditions and Surface Roughness on the Performance of Transitions between Square and Rectangular Ducts of the Same Cross-Sectional Area," *International Journal of Heat and Fluid Flow*, Vol. 8, 1987, pp. 287–292.

[10]Tucker, M. J., and Reynolds, A. J., "The Distortion of Turbulence by Irrotational Plane Stain," *Journal of Fluid Mechanics*, Vol. 32, 1968, pp. 657–673.

[11]Townsend, A. A., "The Uniform Distortion of Homogeneous Turbulence," *Quarterly Journal of Mechanics and Applied Mathematics*, Vol. 7, 1954, pp. 104–127.

[12]Shabaka, I. M. M. A., Mehta, R. D., and Bradshaw, P., "Longitudinal Vortices Imbedded in Turbulent Boundary Layers. Part I: Single Vortex," *Journal of Fluid Mechanics*, Vol. 155, 1985, pp. 37–57.

[13]Miau, J. J., Chou, J. H., Lin, S. F., and Lin, C. K., "Visualization of Flow Near the Wall of a Circular-Rectangular Transition Duct" (in Chinese), *Proceedings of the Fourth National Conference of the Chinese Society of Mechanical Engineering*, Hsinchu, Taiwan, Republic of China, 1987, pp. 83–94.

[14]Tobak, M., and Peake, D. J., "Topology of Three-Dimensional Separated Flows," *Annual Review of Fluid Mechanics*, Vol. 14, 1982, pp. 61–85.

[15]Cebeci, T., and Bradshaw, P., *Momentum Transfer in Boundary Layers*, Hemisphere, Washington, D.C., 1977.

[16]Miau, J. J., Lin, S. A., Chou, J. H., Wei, C. Y., and Lin, C. K., "An Experimental Study of Flow in a Circular-Rectangular Transition Duct," AIAA Paper 88-3029, 1988.

[17]Sovran, G., and Klomp, E. D., "Experimentally Determined Optimum Geometries of Rectilinear Diffusers with Rectangular, Conical or Annual Cross-Section," *Fluid Mechanics of Internal Flow*, edited by G. Sovran, Elsevier, New York, 1967, pp. 271–319.

[18]Burley, J. R. II, and Carlson, J. R., "Circular-to-Rectangular Transition Ducts for High-Aspect Ratio Nonaxisymmetric Nozzles," AIAA Paper 85-1346, 1985.

[19]Towne, C. E., and Schum, E. F., "Application of Computational Fluid Dynamics to Complex Inlet Ducts," AIAA Paper 85-1213, 1985.

[20]Bradshaw, P., "Turbulent Secondary Flows," *Annual Review of Fluid Mechanics*, Vol. 19, 1987, pp. 53–74.

[21]Perkins, H. J., "The Formation of Streamwise Vorticity in Turbulent Flow," *Journal of Fluid Mechanics*, Vol. 44, 1970, pp. 721–740.